J Geophys (1986) 59:129–139

Journal of Geophysics

Interactive high-resolution polarization analysis of broad-band seismograms

A. Plešinger[1], **M. Hellweg**[2] **and D. Seidl**[3]

[1] Geophysical Institute, Czechoslovakian Academy of Sciences, 14131 Praha 4, Czechoslovakia
[2] Institut für Meteorologie und Geophysik, Feldbergstr. 47, D-6000 Frankfurt/M., Federal Republic of Germany
[3] Seismologisches Zentralobservatorium Gräfenberg, Krankenhausstr. 1, D-8520 Erlangen, Federal Republic of Germany

Abstract. In the laterally heterogeneous and anisotropic earth the particle motions of seismic waves are three-dimensionally polarized. This paper presents a method for determining a local wave coordinate system using the zeros of some component operators in rotated systems. It is applicable to broad-band composite waveforms and offers higher precision and resolution for the determination of azimuth and incidence angle than the usual least-squares techniques. The algorithms have been implemented in an interactive program for preprocessing three-component digital recordings. In addition, the program allows the use of particle motion diagrams and component products for the determination of wave types, onset times and pulse durations. Its performance is demonstrated on regional and teleseismic events recorded at the European broad-band stations GRF (Gräfenberg, West Germany), KHC (Kăsperské Hory, Czechoslovakia) and KSP (Ksiaz, Poland).

Key words: Broad-band seismology – Polarization analysis – Azimuth and incidence angle – Particle motion – Component products

Introduction

The seismic wave field is a superposition of many overlapping wave groups: direct, reflected, refracted, converted and scattered body and surface waves. At any point in the earth each wave group has its own shape, velocity and direction. Broad-band stations record the complex local wave field with "high fidelity" as a pronounced multi-pulse seismogram, as compared to the smooth seismograms recorded at narrow-band stations. For further analysis and interpretation, it is essential to separate and identify the various wave groups. This can best be accomplished by a transformation of the seismograms from the coordinate system of the recording seismometers to the apparent local wave coordinate systems of the different wave groups.

At any point on a seismic ray, an intrinsic coordinate system, the Frenet frame, is defined by the basis vectors $\{\mathbf{t}, \mathbf{n}, \mathbf{b}\}$ parallel to the tangent, normal and binormal, respectively (for example, see Aki and Richards, 1980). For a spherically symmetric and isotropic model earth, the tangent $\mathbf{t}$ and the normal $\mathbf{n}$ would be in the plane determined by the source, station and centre of the earth. P waves and S waves would be polarized in the $\mathbf{t}$ direction and in the $\mathbf{n}-\mathbf{b}$ plane, respectively. The Frenet frame could then be determined at a three-component point station using only the polarizations of P and S waves.

In the laterally heterogeneous and anisotropic earth, however, the particle motion of seismic waves is three-dimensionally polarized. Additional criteria are necessary to define a local wave coordinate system, which is no longer directly correlated to the Frenet frame. For narrow-band, quasi-harmonic wave groups an ellipsoidal least-squares fit can be used to determine the local wave coordinate system (for example, see Matsumura, 1981). For broad-band waveforms with arbitrary polarization, an average system can be derived for each wave group from the zeros of some component products and sums in rotated analysis systems. The orientation of the wave system for each wave group in a composite seismogram, described by its azimuth and incidence angle, is important information for the investigation of heterogeneous and anisotropic structures. Furthermore, seismograms, particle motion diagrams and component products calculated in the wave coordinate systems can be used for discrimination of wave type, and for the determination of onset time and estimation of pulse duration.

An interactive procedure for such analysis is demonstrated on regional and teleseismic events recorded at the European broad-band stations GRF (Gräfenberg, West Germany), KHC (Kašperské Hory, Czechoslovakia) and KSP (Ksiaz, Poland).

Apparent local wave coordinate system

Given the seismograms $s_Z(t)$, $s_E(t)$, $s_N(t)$ of a three-component station recording in the right-handed vertical-east-north system with the basis vectors $\{\mathbf{e}_Z, \mathbf{e}_E, \mathbf{e}_N\}$, the orientation of a local wave system with the basis vectors $\{\mathbf{e}_L, \mathbf{e}_Q, \mathbf{e}_T\}$ can be defined by two angles: a and i.

The longitudinal unit vector $\mathbf{e}_L$ (P direction) is given in the recording system by

$$\mathbf{e}_L = (\cos i, -\sin i \sin a, -\sin i \cos a). \quad (1)$$

Offprint requests to: D. Seidl

a ($0° \leqq a \leqq 360°$) is the back-azimuth (to the epicentre) of the projection of $\mathbf{e}_L$ into the horizontal plane against north and i ($0° \leqq i \leqq 90°$ for a station on the earth's surface) is the incidence angle between $\mathbf{e}_L$ and $\mathbf{e}_Z$.

The transverse unit vector $\mathbf{e}_T$ (SH direction) is given by the vector product $\mathbf{e}_L \times \mathbf{e}_Z / |\mathbf{e}_L \times \mathbf{e}_Z|$:

$$\mathbf{e}_T = (0, -\cos a, \sin a). \tag{2}$$

The transverse unit vector $\mathbf{e}_Q$ (SV direction) is determined by the vector product $\mathbf{e}_T \times \mathbf{e}_L$ so that the basis vectors $\{\mathbf{e}_L, \mathbf{e}_Q, \mathbf{e}_T\}$ form a right-handed system. Thus $\mathbf{e}_Q$ becomes

$$\mathbf{e}_Q = (\sin i, \cos i \sin a, \cos i \cos a). \tag{3}$$

The transformation relationship between the seismogram vector $\mathbf{s} = \{s_Z, s_E, s_N\}$ in the recording system and $\mathbf{u} = \{u_L, u_Q, u_T\}$ in the local ray system can be written in matrix notation as

$$\begin{pmatrix} u_L \\ u_Q \\ u_T \end{pmatrix} = \mathbf{M} \begin{pmatrix} s_Z \\ s_E \\ s_N \end{pmatrix} = \begin{pmatrix} \cos i & -\sin i \sin a & -\sin i \cos a \\ \sin i & \cos i \sin a & \cos i \cos a \\ 0 & -\cos a & \sin a \end{pmatrix} \begin{pmatrix} s_Z \\ s_E \\ s_N \end{pmatrix}. \tag{4}$$

The elements in the first, second and third line of the transformation matrix $\mathbf{M}$ are the components of the basis vectors $\{\mathbf{e}_L, \mathbf{e}_Q, \mathbf{e}_T\}$ in the recording system $\{\mathbf{e}_Z, \mathbf{e}_E, \mathbf{e}_N\}$ given in Eqs. (1) through (3).

The inverse relationship to Eq. (4) is given by

$$\begin{pmatrix} s_Z \\ s_E \\ s_N \end{pmatrix} = \mathbf{M}^T \begin{pmatrix} u_L \\ u_Q \\ u_T \end{pmatrix} = \begin{pmatrix} \cos i & \sin i & 0 \\ -\sin i \sin a & \cos i \sin a & -\cos a \\ -\sin i \cos a & \cos i \cos a & \sin a \end{pmatrix} \begin{pmatrix} u_L \\ u_Q \\ u_T \end{pmatrix} \tag{5}$$

where $\mathbf{M}^T$ is the transpose of $\mathbf{M}$.

Determination of azimuth and apparent incidence angle

For azimuth determination the seismogram vector $\mathbf{s}$ is transformed to a vector $\mathbf{v}$ in a rotated analysis system, using Eq. (4) for $i = 90°$ and variable a:

$$\begin{pmatrix} v_R \\ v_Z \\ v_T \end{pmatrix} = \begin{pmatrix} 0 & -\sin a & -\cos a \\ 1 & 0 & 0 \\ 0 & -\cos a & \sin a \end{pmatrix} \begin{pmatrix} s_Z \\ s_E \\ s_N \end{pmatrix} = \begin{pmatrix} -s_E & \sin a - s_N & \cos a \\ & s_Z & \\ -s_E & \cos a + s_N & \sin a \end{pmatrix}. \tag{6}$$

v_R and v_T are the radial and transverse components in the horizontal plane and v_Z is the vertical component of the seismogram vector $\mathbf{v}$ in the rotated analysis system, a is the back-azimuth of the v_R axis.

If a linearly polarized P wave $u_L(t)\,\mathbf{e}_L$ with $i = i_0$ and $a = a_0$ arrives at a seismic station, the seismogram vector $\mathbf{s}$ can be derived from Eq. (5):

$$\begin{pmatrix} s_Z \\ s_E \\ s_N \end{pmatrix} = \mathbf{M}^T \begin{pmatrix} u_L \\ 0 \\ 0 \end{pmatrix} = \begin{pmatrix} \cos i_0 \\ -\sin i_0 \sin a_0 \\ -\sin i_0 \cos a_0 \end{pmatrix} u_L. \tag{7}$$

The vector $\mathbf{v}$ calculated in Eq. (6) will then be:

$$\begin{pmatrix} v_R \\ v_Z \\ v_T \end{pmatrix} = \begin{pmatrix} \cos(a_0 - a) \sin i_0 \\ \cos i_0 \\ \sin(a_0 - a) \sin i_0 \end{pmatrix} u_L. \tag{8}$$

The component products $v_T v_Z$ and $v_R v_Z$ are then:

$$v_T v_Z = u_L^2(t) \sin(a_0 - a) \sin i_0 \cos i_0 \tag{9}$$

$$v_R v_Z = u_L^2(t) \cos(a_0 - a) \sin i_0 \cos i_0. \tag{10}$$

A SV wave $u_Q(t)\,\mathbf{e}_Q$ with $i = i_0$ and $a = a_0$ can be described using Eq. (5):

$$\begin{pmatrix} s_Z \\ s_E \\ s_N \end{pmatrix} = \mathbf{M}^T \begin{pmatrix} 0 \\ u_Q \\ 0 \end{pmatrix} = \begin{pmatrix} \sin i_0 \\ \cos i_0 \sin a_0 \\ \cos i_0 \cos a_0 \end{pmatrix} u_Q. \tag{11}$$

Inserting Eq. (11) into Eq. (6) the vector $\mathbf{v}$ will be:

$$\begin{pmatrix} v_R \\ v_Z \\ v_T \end{pmatrix} = \begin{pmatrix} -\cos(a_0 - a) \cos i_0 \\ \sin i_0 \\ -\sin(a_0 - a) \cos i_0 \end{pmatrix} u_Q. \tag{12}$$

The component products $v_T v_Z$ and $v_R v_Z$ are then given by

$$v_T v_Z = -u_Q^2(t) \sin(a_0 - a) \cos i_0 \sin i_0, \tag{13}$$

$$v_R v_Z = -u_Q^2(t) \cos(a_0 - a) \cos i_0 \sin i_0. \tag{14}$$

The product $v_T v_Z$ has a zero with regard to a at a_0 for both linearly polarized P waves and SV waves and can therefore be used as an operator for the determination of the azimuth a_0.

For a SH wave, $u_T(t)\,\mathbf{e}_T$ with $i = i_0$ and $a = a_0$, Eq. (5) gives:

$$\begin{pmatrix} s_Z \\ s_E \\ s_N \end{pmatrix} = \mathbf{M}^T \begin{pmatrix} 0 \\ 0 \\ u_T \end{pmatrix} = \begin{pmatrix} 0 \\ -\cos a_0 \\ \sin a_0 \end{pmatrix} u_T. \tag{15}$$

Inserting Eq. (15) into Eq. (6) it follows for the vector $\mathbf{v}$:

$$\begin{pmatrix} v_R \\ v_Z \\ v_T \end{pmatrix} = \begin{pmatrix} -\sin(a_0 - a) \\ 0 \\ \cos(a_0 - a) \end{pmatrix} u_T. \tag{16}$$

The component products $v_T v_Z$ and $v_R v_Z$ are given by

$$v_T v_Z = 0, \tag{17}$$

$$v_R v_Z = 0. \tag{18}$$

For a sinusoidal Rayleigh-wave ($\varepsilon_0 \cos\omega t$, $\varepsilon_0 \sin\omega t, 0$) with surface ellipticity ε_0 (ratio of horizontal to vertical amplitudes) and back-azimuth a_0, Eq. (5) gives, with $i_0 = 90°$:

$$\begin{pmatrix} s_Z \\ s_E \\ s_N \end{pmatrix} = \mathbf{M}^T \begin{pmatrix} u_L \\ u_Q \\ 0 \end{pmatrix} = \begin{pmatrix} \sin\omega t \\ -\varepsilon_0 \sin a_0 \cos\omega t \\ -\varepsilon_0 \cos a_0 \cos\omega t \end{pmatrix}. \tag{19}$$

Inserting Eq. (19) into Eq. (6) it follows:

$$\begin{pmatrix} v_R \\ v_Z \\ v_T \end{pmatrix} = \begin{pmatrix} \varepsilon_0 \cos(a_0 - a) \cos\omega t \\ \sin\omega t \\ \varepsilon_0 \sin(a_0 - a) \cos\omega t \end{pmatrix}. \tag{20}$$

The component product $v_R v_Z$ is given by

$$v_R v_Z = 0.5\, \varepsilon_0 \cos(a_0 - a) \sin 2\omega t. \tag{21}$$

For Love-waves $(0, 0, u_T)$, the component product $v_R v_Z$ is given by Eq. (18).

As a function of time, the component product $v_R v_Z$ is therefore always positive for P waves [Eq. (10)], negative for SV waves [Eq. (14)] and zero for SH and Love waves [Eq. (18)]. For Rayleigh waves, $v_R v_Z$ oscillates between positive and negative values with frequency 2ω for sinusoidal Rayleigh waves of frequency ω [Eq. (21)]. $v_R v_Z$ can therefore be used as an operator for wave type discrimination. (REMODE-Filter; for example, see Kanasewich, 1981).

The ground motion generated by an incident body wave at the free surface is a superposition of three waves: the incident P or S wave, the reflected P or S wave and the converted S or P wave. The displacement recorded by a three-component station thus differs from that of the incident wave. For linearly polarized incident P waves the particle motion remains linear in the plane of incidence for any angle of incidence. For linearly polarized S waves with an under-critical angle of incidence, all three components are in phase and the resultant particle motion remains linear. In the over-critical case the components are out of phase and the resultant motion becomes three-dimensional. The relationships between the apparent and true angle are expressed by conversion formulas published, for example, by Nuttli and Whitmore (1961). A practical application of the conversion formulas is epicentre location with a single three-component station. For the inversion of seismograms and particle motion diagrams with synthetics, the conversion at the earth's surface is incorporated in the numerical algorithm.

To determine the apparent angle of incidence, the seismogram vector **s** is transformed to a vector **v'** in a rotated analysis system, using $a = a_0$ and $i' = i + 45°$ in Eq. (4):

$$\begin{pmatrix} v'_L \\ v'_Q \\ v'_T \end{pmatrix} = \begin{pmatrix} s_Z \cos i' + v_R \sin i' \\ s_Z \sin i' - v_R \cos i' \\ -s_E \cos a_0 + s_N \sin a_0 \end{pmatrix} \tag{22}$$

where v_R is calculated from Eq. (6) for $a = a_0$. Inserting Eq. (7) for a linearly polarized P wave into Eq. (22) and using Eq. (6) for v_R and $a = a_0$, the component difference $v'_L - v'_Q$ is given by

$$v'_L - v'_Q = \sqrt{2}\, u_L \sin(i_0 - i). \tag{23}$$

Using Eq. (11) for a SV wave, it then follows in the same way for the component sum $v'_L + v'_Q$:

$$v'_L + v'_Q = \sqrt{2}\, u_Q \sin(i_0 - i). \tag{24}$$

In terms of the rotation angle i, the component difference $v'_L - v'_Q$ and the component sum $v'_L + v'_Q$ have zeros at $i = i_0$ for linearly polarized P waves and SV waves, respectively, and can therefore be used as operators for the determination of the apparent incidence angle i_0.

Interactive analysis

An efficient application of the algorithm is provided by an interactive program using a graphics terminal. Analysis takes place in two steps. First, the azimuth and apparent angle of incidence are determined for each wave group using component operators. Then the seismograms are calculated in the wave coordinate systems and plotted along with particle motion diagrams and the component products.

The component operators yielding the best resolution for the determination of azimuth, incidence angle and onset time are summarized in Table 1. Corresponding to Eqs. (9) and (13), the component product $v_T v_Z$, calculated for linearly polarized P waves and pure SV waves using Eq. (6), changes sign if the azimuth of the rotated system passes the wave azimuth a_0. If the P or SV wave is non-linearly polarized, the change of first-motion sign of $v_T v_Z$ determines the first-motion azimuth. The average azimuth is defined by the condition $\int v_T(a)\, v_Z\, dt = 0$, where the integration interval can be obtained from the pulse duration of the component product $v_R(a)\, v_Z$. In the same way, the first-motion and average incidence angles for P and SV waves can be determined using $v'_L - v'_Q$ [Eq. (23)] and $v'_L + v'_Q$ [Eq. (24)], respectively.

After the determination of azimuth and apparent incidence angle, seismograms and component products are calculated in the $L-Q-T$ wave system using Eq. (4). They can be displayed along with particle motion diagrams on a graphics terminal. It is also possible to identify and mark phases and to measure onset-times on seismogram traces as well as particle motion diagrams and component products. Marked times can be indicated in the other representations.

Table 1. Component operators for polarization analysis

Determination of	Wave type	Component operator
Azimuth a_0	P, SV	$v_T(a) \cdot v_Z$
Apparent	P	$v'_L(a_0, i) - v'_Q(a_0, i)$
Incidence angle i_0	SV	$v'_L(a_0, i) + v'_Q(a_0, i)$
Onset time	P	$v_R(a_0) \cdot v_Z$
Pulse duration	SV	
Wave type	SH	$v_T(a_0)$

Examples

The polarization analysis is demonstrated on digital broad-band recordings of events from Hokkaido, Afghanistan, the Aegean Sea and the Swabian Jura. The hypocentral and station parameters are summarized in Table 2. The digital recordings of stations KHC (Kašperské Hory) and KSP (Ksiaz) are proportional to displacement in the period range from T_L to T_U given in Table 2. They were obtained from the original analog (FM) broad-band velocity-proportional magnetic tape recordings by analog filtering (Plešinger and Horálek, 1976) and computer-aided A/D conversion (Plešinger, 1981). The displacement seismograms of stations GRFA1 and GRFB1 of the Gräfenberg array (Harjes and Seidl, 1978; Seidl and Stammler, 1984) are calculated from the original broad-band velocity-proportional recordings by digital restoration filtering (Seidl, 1980) for the period band T_L to T_U.

Figures 1–3 present the analysis of the multi-pulse *P* wave group of the Hokkaido event, recorded at station KHC.

Figure 1a shows the horizontal particle motion diagrams for successive 13.4-s time intervals. The first diagram begins with a nearly linearly polarized pulse, followed by signals with highly irregular two-dimensional polarization patterns. In Fig. 1b the component product $v_T(a)v_Z$ is plotted for various values of the azimuth a. The onset of $v_T v_Z$ changes its sign for an azimuth in the interval [38°, 39°]. This value is the first-motion azimuth, corresponding to the slope of the tangent on the particle motion diagram at the onset time. The average azimuths of the two-dimensionally polarized wave groups *P*, *P1* and *P2* are determined by the condition $\int v_T(a)v_Z\,dt=0$, where the integration intervals are obtained from the component product *RZ*.

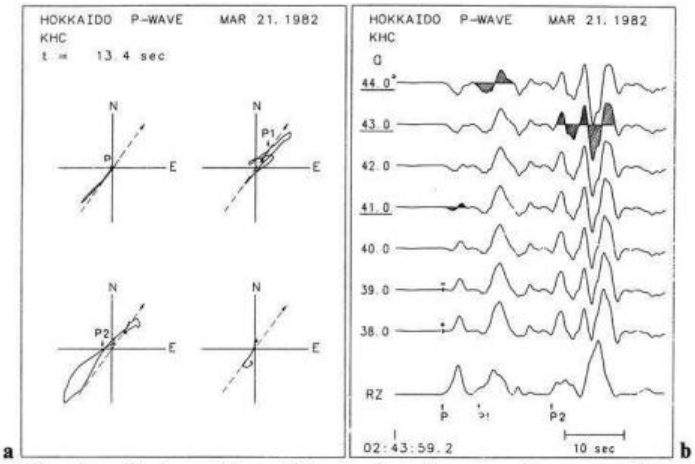

Fig. 1. a Horizontal particle motion diagrams in consecutive 13.4-s intervals for the composite *P* wave group of the Hokkaido event in Table 2. The *triangles* mark the beginning of the intervals. The *dashed line* is the great circle direction towards the epicentre. The *arrows* indicate the onsets of the pulses marked on the *RZ* trace in **b**. **b** $v_T(a)v_Z$ traces for the determination of the average azimuths a of the pulses indicated using the condition $\int v_T(a)v_Z\,dt=0$. The integration intervals, indicated by the *hatched areas*, are obtained from the product *RZ* plotted for the azimuth $a=41°$. The first-motion azimuth, indicated by the change of sign, is in the interval [38°, 39°]

Table 2. Hypocentral and station parameters for the events analysed

Hypocentral data							Station data				
Location	Date	Origin time	Latitude (N)	Longitude (E)	Depth (km)	$\frac{m_b}{M_S}$	Station (T_L, T_U)	Epicentral distance (degrees)	Azimuth (degrees N)	Incidence angle[a] (degrees)	
										P	*S*
Swabian Jura	Sep 03 1978	05:08:30.7	48.34	9.14	6	$\frac{4.9}{5.3}$	GRFA1 (1, 25)	1.9	226.2	(50)	(50)
							GRFB1 (1, 25)	2.0	238.6	(50)	(50)
							KHC (0.25, 60)	3.0	256.6	(50)	(50)
Afghanistan – USSR Border Region	May 02 1981	16:04:54.6	36.40	71.15	223	5.9 –	GRFA1 (1, 60)	44.6	83.8	25	26
							KHC (0.5, 150)	43.1	84.8	26	26
Aegean Sea	Dec 19 1981	14:10:51.1	39.22	25.25	16	$\frac{6.0}{7.2}$	KSP (0.3, 280)	13.2	148.1	(50)	(50)
Hokkaido	Mar 21 1982	02:32:05.9	42.23	142.46	36	$\frac{6.3}{6.9}$	KHC (0.3, 280)	78.5	36.2	17	19

[a] The theoretical incidence angles are taken from Pho and Behe (1972) and Chandra (1972). The values in parentheses are estimations for a single layer crustal model

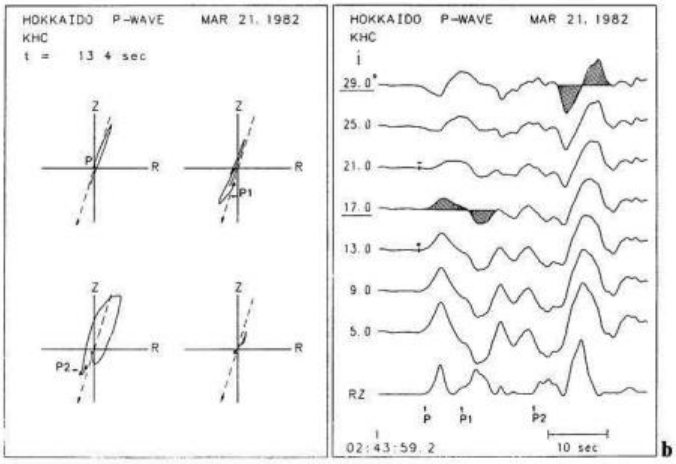

Fig. 2. **a** Particle motion diagrams in the $R-Z$ (radial-vertical) plane for $a=41°$. The *dashed line* indicates the theoretical incidence angle, $i_0=17°$. **b** $v'_L-v'_Q$ traces for the determination of the average apparent incidence angle i for the P wave group shown in Fig. 1 using the condition $\int [v'_L(a,i) - v'_Q(a,i)]\,dt=0$. Integration intervals and labels as in Fig. 1b. The first-motion and average apparent incidence angles are in the same interval, [15°, 19°]

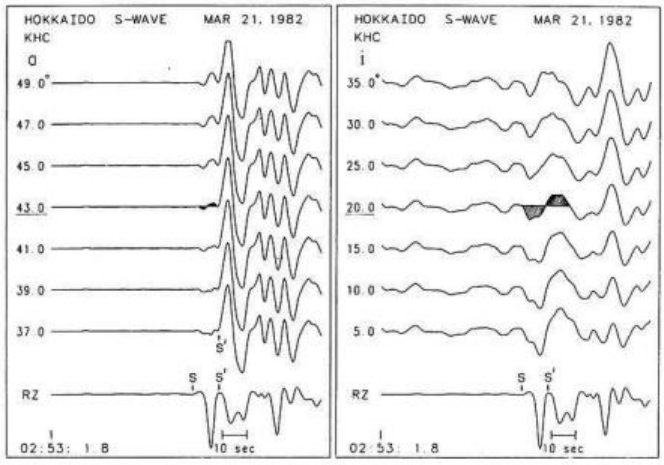

Fig. 4. $v_T(a)\,v_Z$ and $v'_L(a,i)+v'_Q(a,i)$ traces for the determination of average azimuth a and average apparent incidence angle i for the S wave group of the Hokkaido event using the conditions $\int v_T v_Z\,dt=0$ and $\int (v'_L+v'_Q)\,dt=0$. The *arrow* labelled S on the RZ trace indicates the Jeffreys-Bullen arrival time. The tiny positive initial pulse results from using the average wave-group azimuth to compute v_R rather than the azimuth determined by the first onset

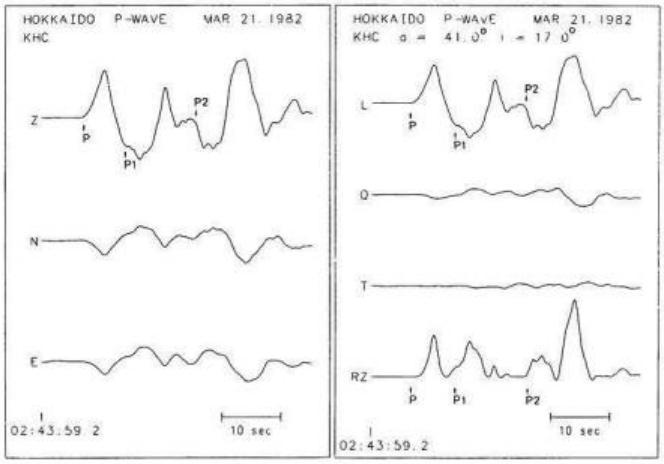

Fig. 3. Displacement recordings for the P wave group of the Hokkaido event and the seismograms transformed into the $L-Q-T$ system for $a=41°$ and $i=17°$ together with the RZ product

The value of the integral changes its sign in the interval [40.5°, 41.5°] for the P pulse. For the pulses $P1$ and $P2$, the intervals are [43°, 45°] and [42°, 44°], respectively. The great circle azimuth is 36°.

Figure 2a shows the corresponding particle motion diagrams in the vertical-radial plane for azimuth $a=41°$ of the first P pulse. Again, the polarization of the first pulse is nearly linear, followed by signals with two-dimensional polarization patterns. Figure 2b shows the component differences $v'_L-v'_Q$ for various incidence angles i. The average incidence angle for P and $P1$ is in the interval [15°, 19°], and for $P2$ in the interval [28°, 30°]. The true angle of incidence, taken from the tables from Pho and Behe (1972), is 17°.

Figure 3 shows the original recordings as well as the seismograms transformed into the $L-Q-T$ coordinate system for azimuth $a=41°$ and incidence angle $i=17°$ together with the RZ product. The polarization is mainly linear in the L direction with slight contamination visible on the Q and T components. This is due to the non-linearity of the polarization and the variations in the azimuth and incidence angle for the incoming wavefront as a function of time. Thus, the P wave group consists of at least three different pulses. The onset times for $P1$ and $P2$ are best measured using the RZ trace.

The analysis of the S wave group of the Hokkaido event is presented in Figs. 4 and 5. The $v_T v_Z$ traces in Fig. 4 indicate a multiple wave group with an average azimuth in the interval [42°, 44°] for the first pulse. The diagrams of the component sum $v'_L+v'_Q$ have no clear multiple waveform. The average incidence angle is in the interval [18°, 22°] for the first pulse. The $L-Q-T$ seismograms, component products and particle motion diagrams in Fig. 5 exhibit clear S-wave splitting, which cannot be resolved in the original three-component recordings. The wave group begins with a SV-polarized pulse S, followed by a wave group S' with SV and SH components 7.8 s later. The pulses with SV components can be recognized using the RZ component product. The arrows indicate the JB arrival times of phases S, SKS and ScS. The transition from SV- to SH-polarization can be seen exceptionally clearly in the $Q-T$ particle motion diagram. An additional clear onset labelled SKS can be recognized in the $Q-L$ and $L-T$ diagrams. Generally, first-motion onset times can best be measured using the $L-Q-T$ seismograms. For later phases, the products TZ and RZ used in conjunction with the $L-Q-T$ diagrams produce higher accuracy and resolution for arrival time readings.

Figure 6 presents the analysis of the composite P wave group of the event in the Aegean Sea region, recorded at station KSP. The average azimuth for the complete wave group is in the interval [149.5°, 150.5°].

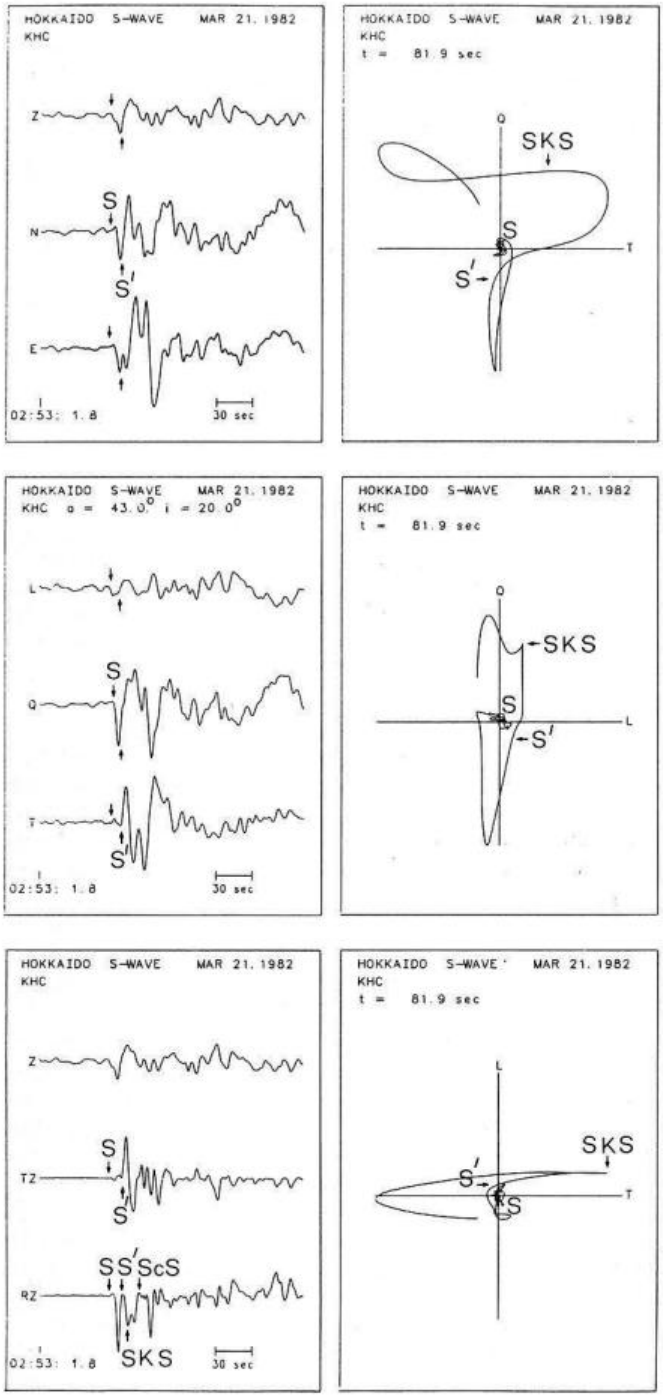

Fig. 5. Displacement recordings and component products as well as seismograms and particle motion diagrams in the $L-Q-T$ system for the S wave group of the Hokkaido event. The most interesting feature is the resolution of wave splitting in the first S pulse, labelled S and S'. The *arrows* on the RZ trace indicate the Jeffreys-Bullen arrival times of S, SKS and ScS

Within the time window of the first RZ pulse, $v'_L - v'_Q$ changes sign in the interval [44°, 48°] for the apparent incidence angle. The values for the great circle azimuth and the true angle of incidence are 148° and about 50° for a standard earth model. The seismograms and particle motion diagrams in the corresponding $L-Q-T$ system reveal pronounced P-wave splitting. The L trace begins with a linearly polarized P pulse, followed by a signal P' with SV-polarization on the Q trace. The delay in the onset times is 4.8 s. The SH contaminations on the T trace are very small during the time interval analysed. This splitting can also be seen in the polarization diagrams for the $Q-L$ and $L-T$ planes, plotted for the first 54.4-s time segment. The P pulse duration is 12.3 s, measured on the RZ trace. The P pulse is followed by a PL mode with regular dispersion in the period interval from about 60 to 30 s. Superimposed on this mode is a high-frequency P wave group $P1$, interpreted by Rademacher et al. (1983) as the $P-P$ reflection from the 400-km discontinuity.

Figures 7 and 8 show the seismograms and particle motion diagrams of the Love-Rayleigh wave segment of the earthquake in the Aegean Sea region. The ground motion consists of a regularly dispersed Love wave on the T trace with three superimposed Rayleigh wave groups. The onset of the first wave group R is indicated by the RZ product. The onsets of the multi-pathing wave groups R' and R'' can be determined best from the particle motion diagrams.

Figures 9 and 10 present the analysis of the P wave group of an intermediate-depth earthquake in the Afghanistan region, recorded at stations KHC and GRFA1. The first sections of the particle motion diagrams are nearly linearly polarized, followed by coda waves with irregular two-dimensional polarization patterns. The intervals for the azimuth and the apparent incidence angle are [88.75°, 89.25°] and [25°, 27°] for KHC, [89.25°, 89.75°] and [29°, 31°] for GRFA1. The values for the great circle azimuth and the true incidence angle are given in Table 2. The seismograms and component products are summarized in Fig. 10. The low-frequency part of the seismograms is linearly polarized with little contamination in the Q and T components. The superimposed high-frequency wave groups show enhanced amplitudes in the GRFA recordings with irregular polarization pattern, indicated by the contamination in the Q and T components and by the component products QT, LT and LQ. The onset times of the various overlapping pulses can best be measured using the RZ trace. The theoretical arrival times are labelled for some phases.

As an example for a near event, Figs. 11–13 show the analysis of the Pn wave group of the Swabian Jura earthquake on September 3, 1978, recorded at stations GRFA1, GRFB1 and KHC. The displacement seismograms have a double-pulse waveform. The second pulse was identified by Kind (1979) as being sPn. At station GRFA1, the azimuth for the Pn and sPn pulses are in the intervals [231°, 233°] and [225°, 227°], respectively. The interval for the apparent incidence angle is [53°, 57°] for both phases. The most astonishing feature apparent in the particle motion diagrams is the nearly circular polarization in the radial-vertical plane for both Pn and sPn. The seismograms in the $L-Q-T$ system reveal that this polarization patterns is caused by a pulse on the Q component with a signal form approaching the time derivative of the L-component seismogram. This effect is also visible but less pronounced on the GRFB1 recordings shown in Fig. 12. Possible explanations include wave propagation through anisotropic layers and near-field terms. At

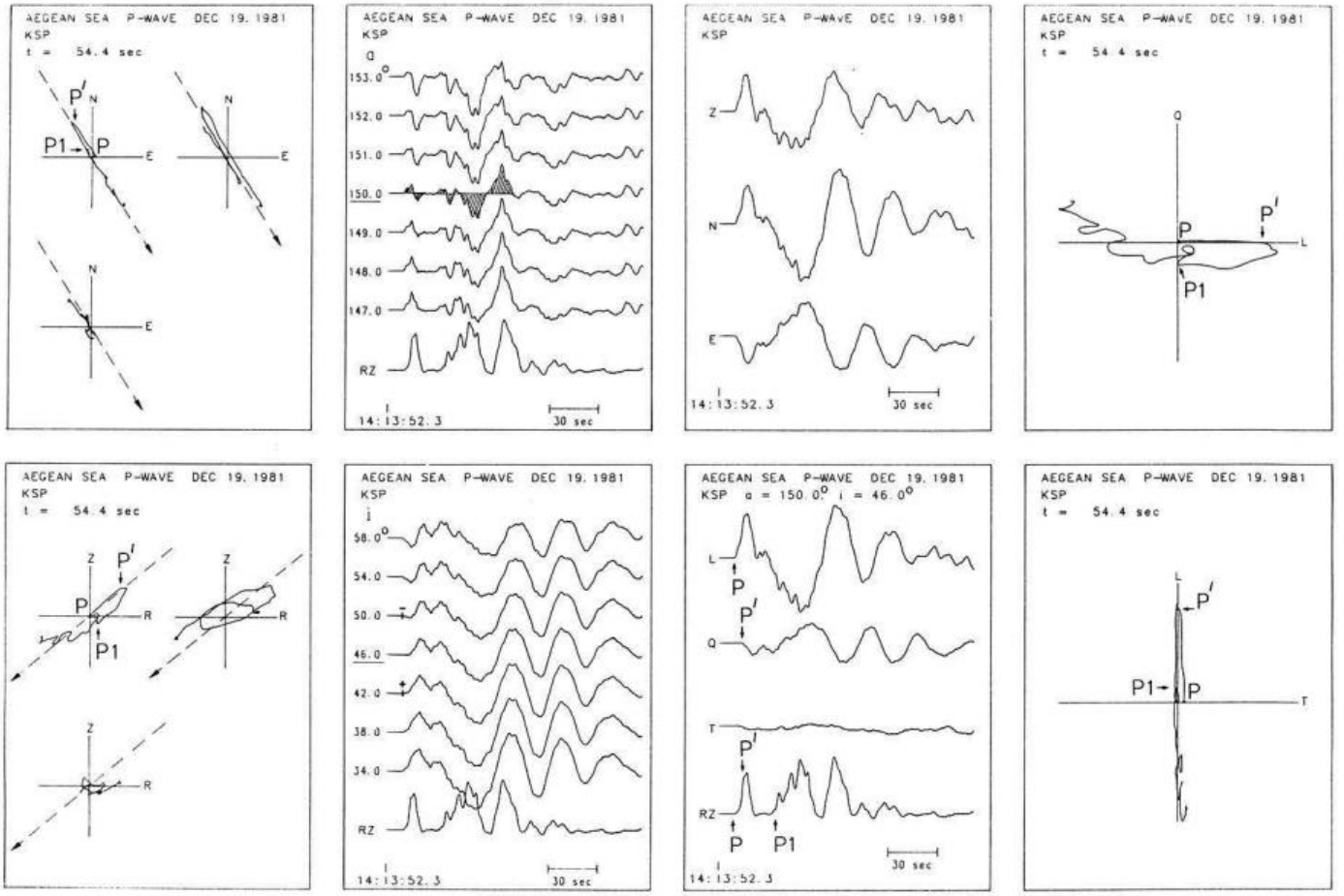

Fig. 6. Analysis of the composite P wave group for the Aegean Sea event in Table 2. The determination of azimuth and apparent incidence angle is analogous to Fig. 1. The seismograms and particle motion diagrams in the $L-Q-T$ system reveal wave splitting in the first P pulse, labelled P and P'. The high-frequency phase $P1$, superimposed on the long-period PL mode, was interpreted by Rademacher et al. (1983) as the $P-P$ reflection from the 400-km discontinuity

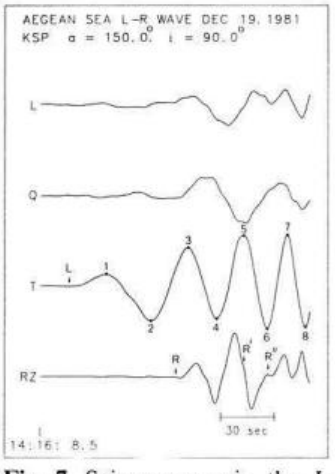

Fig. 7. Seismograms in the $L-Q-T$ system and RZ component product for the Love-Rayleigh wave segment of the Aegean Sea event with labelled onsets of the Love wave and the three Rayleigh wave groups R, R' and R''

KHC (Fig. 13) the Q component has no "derivative" signal form. Both the Pn and sPn pulses are nonlinearly polarized in the horizontal plane, and the polarization anomaly in the radial-vertical ($R-Z$) plane is considerably less pronounced.

Conclusions

Broad-band recordings of seismic waves are composite waveforms, generated by multiple events, multi-path propagation, conversion and wave splitting in the laterally heterogeneous and anisotropic earth. A procedure for the time-domain analysis of digital three-component broad-band recordings using seismograms, particle motion diagrams and component products in rotated coordinate systems has been described. The orientations for these systems are determined using the zeros of wave-type-dependent component operators. In comparison to standard methods, such as ellipsoidal least-squares fits of narrow-band particle motion diagrams (for example, see Matsumara, 1981), the method

(1) is applicable to composite waveforms with arbitrary three-dimensional polarization,

(2) offers higher precision and resolution for the determination of azimuth, incidence angle, onset time and pulse duration, and

(3) gives azimuth and incidence angle as intervals instead of mean values with standard errors.

The procedure has been demonstrated using broad-band displacement seismograms of regional and teleseismic events. The results, although presented phenomenologically without interpretation, illustrate the useful-

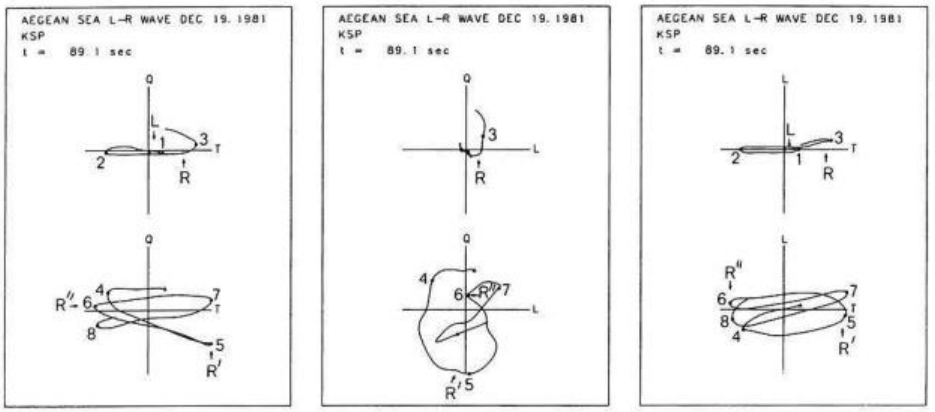

Fig. 8. Particle motion diagrams in the $L-Q-T$ system for the Love-Rayleigh wave segment in Fig. 7. The *numbers* indicate the times of the maxima and minima of the T trace in Fig. 7

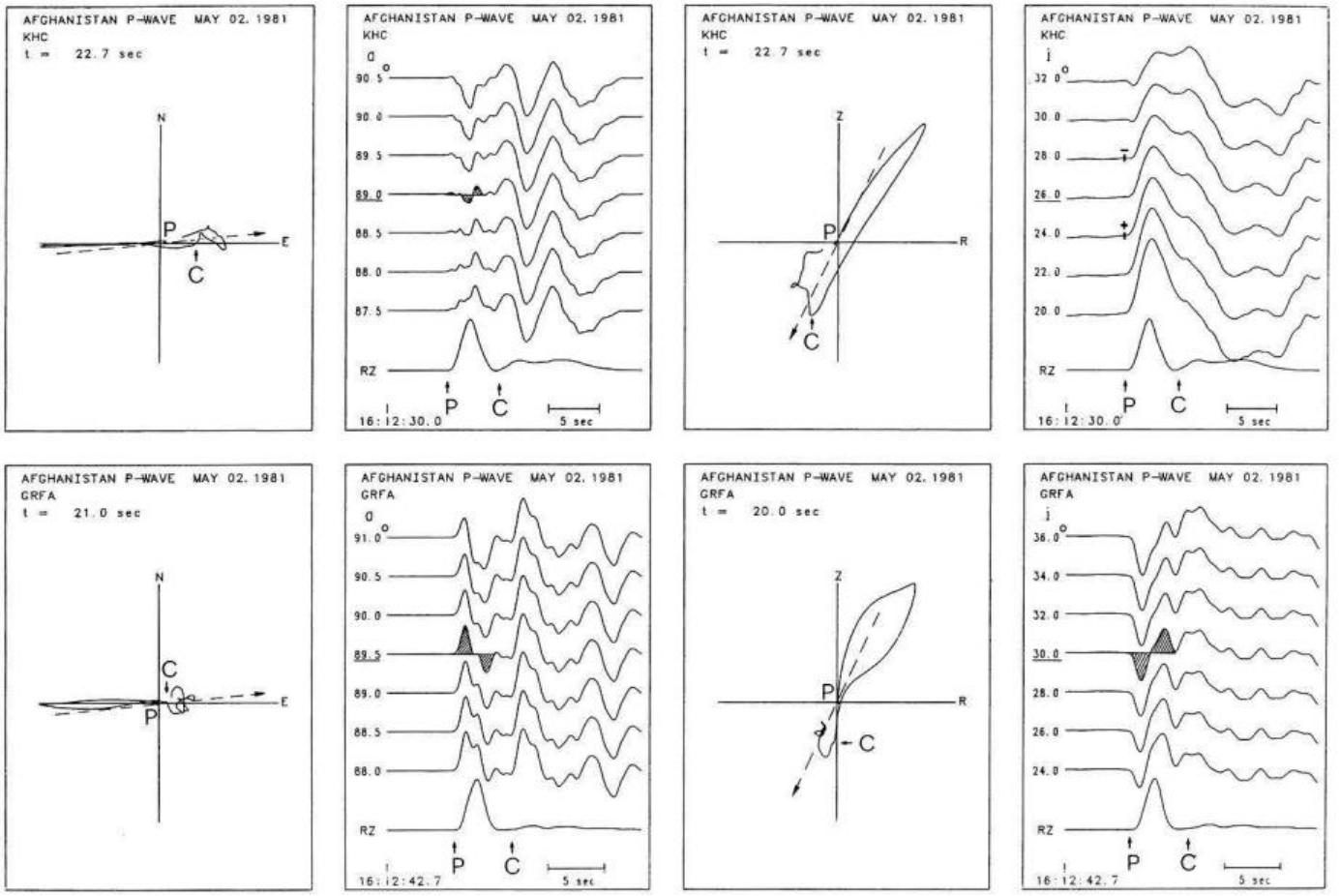

Fig. 9. Determination of azimuth and apparent incidence angle for the P wave group of an intermediate-depth-focus earthquake in the Afghanistan region, recorded at stations KHC and GRFA1. The hypocentre and station parameters are given in Table 2

Fig. 10. Displacement recordings as well as seismograms and component products in the $L-Q-T$ system for the Afghanistan earthquake. The *arrows* on the RZ trace indicate the theoretical arrival times for the labelled phases

Fig. 11. Determination of azimuth and apparent incidence angle as well as displacement recordings and $L-Q-T$ seismograms for the $Pn-sPn$ phases of the Swabian Jura earthquake in Table 2, recorded at station GRFA1. The most interesting feature is the nearly circular polarization of both phases in the vertical-radial plane. Note the sharp onset of sPn on the RZ trace

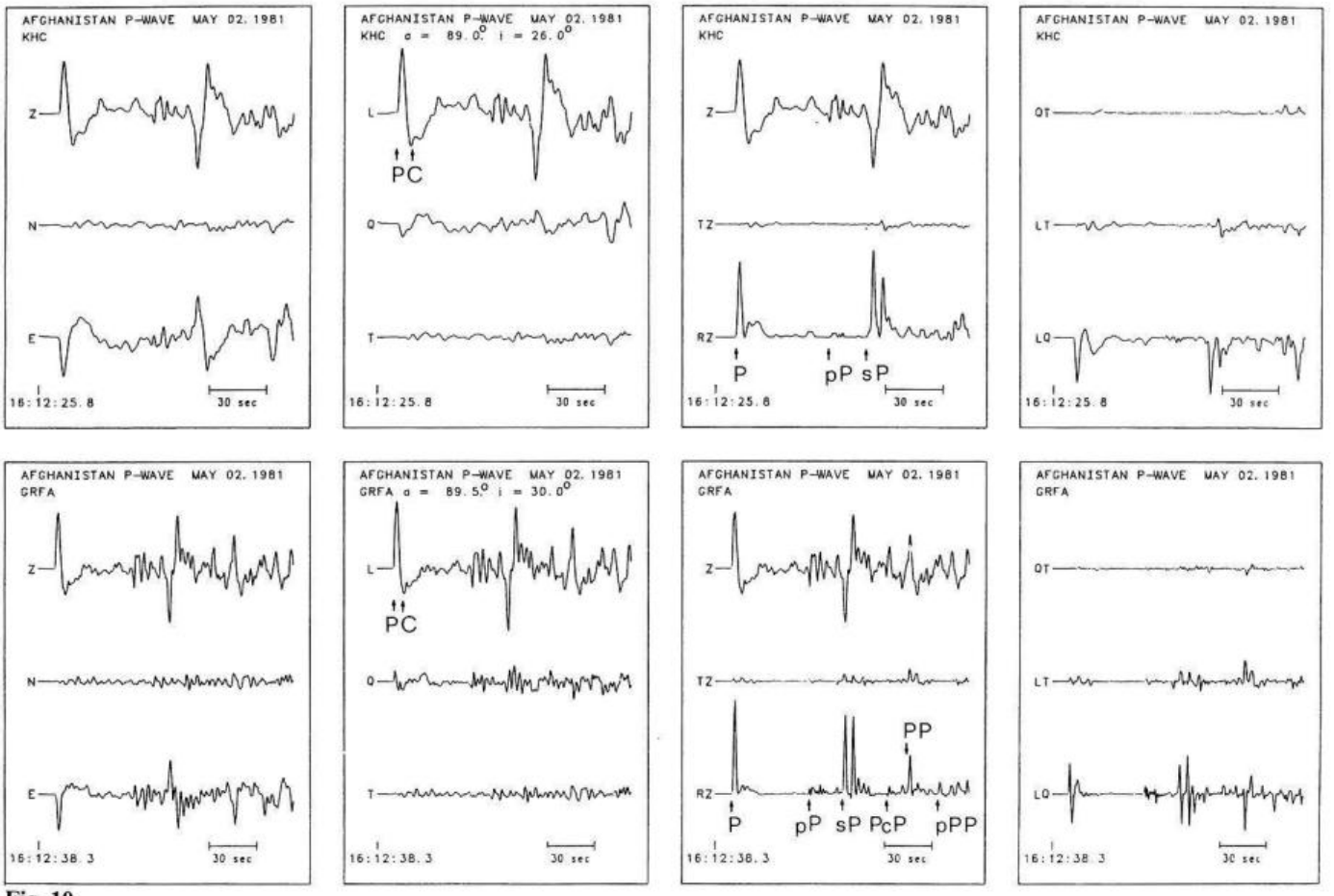
AFGHANISTAN P-WAVE MAY 02. 1981
KHC
Z
N
E
16:12:25.8
30 sec
AFGHANISTAN P-WAVE MAY 02. 1981
KHC a = 89.0° i = 26.0°
L
PC
Q
T
16:12:25.8
30 sec
AFGHANISTAN P-WAVE MAY 02. 1981
KHC
Z
TZ
RZ
P
pP sP
16:12:25.8
30 sec
AFGHANISTAN P-WAVE MAY 02. 1981
KHC
QT
LT
LQ
16:12:25.8
30 sec
AFGHANISTAN P-WAVE MAY 02. 1981
GRFA
Z
N
E
16:12:38.3
30 sec
AFGHANISTAN P-WAVE MAY 02. 1981
GRFA a = 89.5° i = 30.0°
L
PC
Q
T
16:12:38.3
30 sec
AFGHANISTAN P-WAVE MAY 02. 1981
GRFA
Z
TZ
RZ
PP
P
pP sP PcP
pPP
16:12:38.3
30 sec
AFGHANISTAN P-WAVE MAY 02. 1981
GRFA
QT
LT
LQ
16:12:38.3
30 sec

Fig. 10

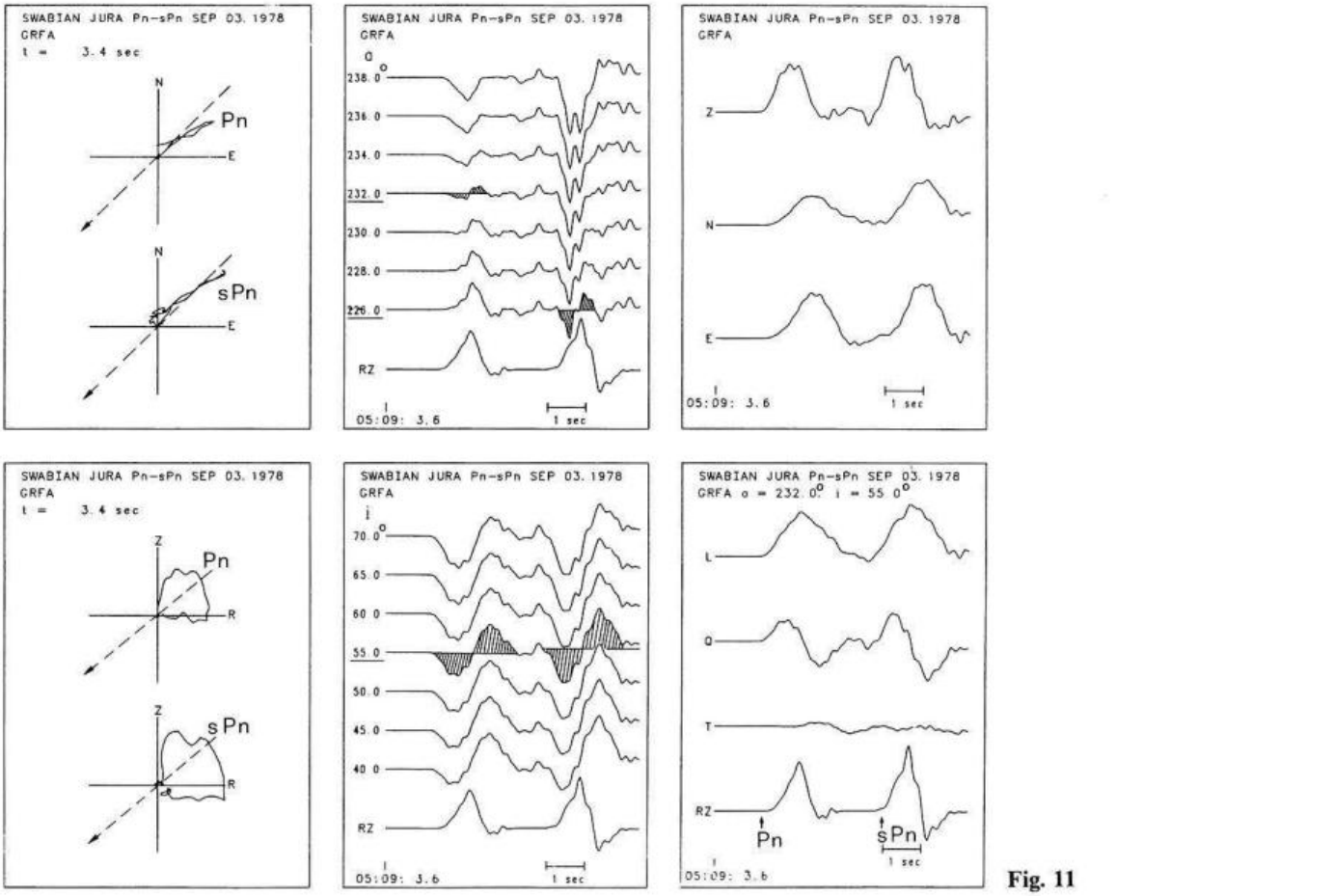
SWABIAN JURA Pn-sPn SEP 03. 1978
GRFA
t = 3.4 sec
N
Pn
E
N
sPn
E
SWABIAN JURA Pn-sPn SEP 03. 1978
GRFA
Q
238.0°
236.0
234.0
232.0
230.0
228.0
226.0
RZ
05:09: 3.6
1 sec
SWABIAN JURA Pn-sPn SEP 03. 1978
GRFA
Z
N
E
05:09: 3.6
1 sec
SWABIAN JURA Pn-sPn SEP 03. 1978
GRFA
t = 3.4 sec
Z
Pn
R
Z
sPn
R
SWABIAN JURA Pn-sPn SEP 03. 1978
GRFA
i
70.0°
65.0
60.0
55.0
50.0
45.0
40.0
RZ
05:09: 3.6
1 sec
SWABIAN JURA Pn-sPn SEP 03. 1978
GRFA a = 232.0° i = 55.0°
L
Q
T
RZ
Pn
sPn
05:09: 3.6
1 sec

Fig. 11

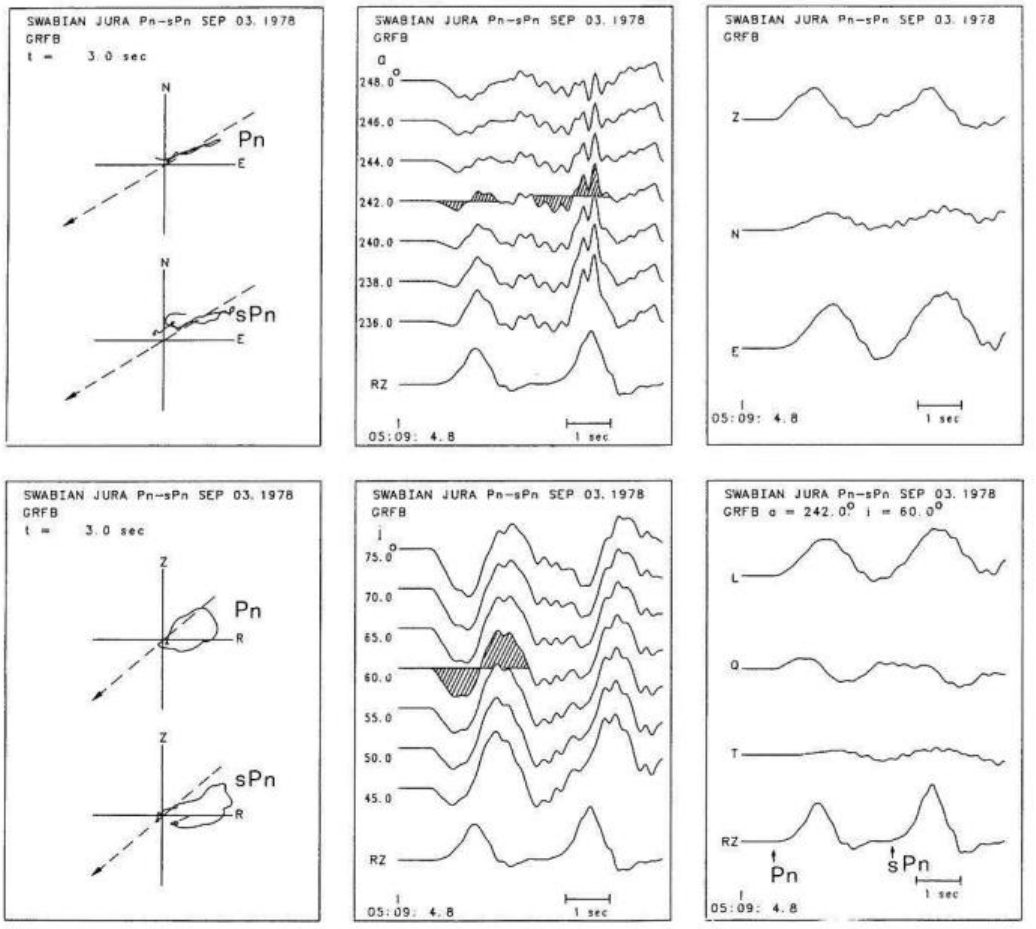

Fig. 12. Analysis of the $Pn-sPn$ wave group of the Swabian Jura earthquake recorded at station GRFB1

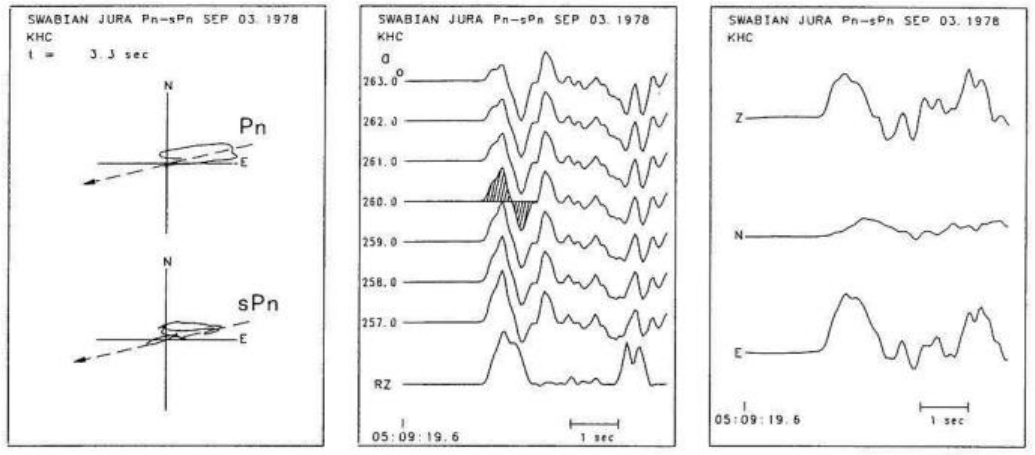

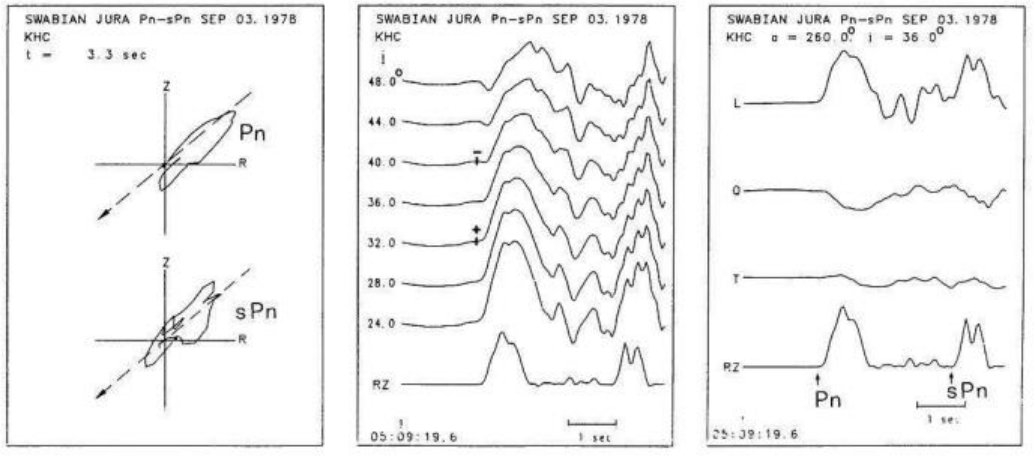

Fig. 13. Analysis of the $Pn-sPn$ wave group of the Swabian Jura earthquake recorded at station KHC

ness of polarization analysis for source studies and structural investigations. From the variety of applications the following should be mentioned:

As has been demonstrated by Brüstle (1985), modelling of complex, multiple sources from broadband recordings is performed best in the time domain. Seismogram pre-processing by polarization analysis provides criteria for the decomposition of composite waveforms into single pulses and for the determination of wave parameters such as pulse duration and displacement time integrals.

For the modelling of laterally heterogeneous structures, the input data are anomalies of onset times, azimuths and incidence angles with regard to a three-dimensional model earth. These data can be measured for the different pulses of a composite waveform using seismograms, particle motion diagrams and component products in properly rotated coordinate systems. As a special result, it has been found that the azimuth anomalies with respect to a spherically homogeneous earth are usually small compared to the anomalies for the incidence angle. This result has been confirmed for *S* waves by numerical experiments performed by Cormier (1984).

The most important application of polarization analysis of three-component broad-band seismograms is likely to be the investigation of anisotropic structures, especially when combined with digital band-pass frequency filtering (Bamford, 1977; Crampin et al., 1984). In anisotropic media, both body and surface waves are three-dimensionally polarized (Crampin, 1977; Keith and Crampin, 1977a, b, c). Rotated seismograms, particle motion diagrams and component products enable the resolution of wave splitting, and aid in the investigation of the fine structure of "quasi-P" and "quasi-*S*" waves as well as different types of "inclined", "tilted" and "sloping" Rayleigh waves.

Acknowledgements. The authors are greatly indebted to Dr. Ivan Pšenčik for stimulating discussions. One of the authors (A.P.) thanks the German Research Council and the University of Stuttgart for enabling him to carry out the present study during his stay at the Geophysical Institute, and the Federal Institute for Geosciences and Natural Resources in Hannover for providing the necessary facilities at the Central Seismological Observatory Gräfenberg in Erlangen. The study is also part of a research project of the Institute for Geophysics and Meterology of the University of Frankfurt supported by the German Research Council.

References

Aki, K., Richards, P.G.: Quantitative seismology, pp. 103–104. San Francisco: Freeman 1980

Bamford, D.: Seismic anisotropy – the state of the art. Geophys. J. **49**, 1–8, 1977

Brüstle, W.: Der Bruchvorgang im Erdbebenherd – Untersuchung ausgewählter Erdbeben mit beobachteten und synthetischen Seismogrammen. Berichte des Instituts für Meteorologie und Geophysik der Universität. Frankfurt/M., Nr. 63, 1985

Chandra, U.: Angles of incidence of S waves. Bull. Seismol. Soc. Am. **62**, 903–915, 1972

Cormier, V.F.: The polarization of S waves in a heterogeneous isotropic earth model. J. Geophys. **56**, 20–23, 1984

Crampin, S.H.: A review of the effects of anisotropic layering on the propagation of seismic waves. Geophys. J. **49**, 9–27, 1977

Crampin, S., Chesnokov, E.M., Hipkin, R.G.: Seismic anisotropy – the state of the art: II. Geophys. J. **76**, 1–16, 1984

Harjes, H.-P., Seidl, D.: Digital recording and analysis of broad-band seismic data at the Graefenberg (GRF)-array. J. Geophys. **44**, 511–523, 1978

Kanasewich, E.R.: Time sequence analysis in geophysics, 3rd ed. Alberta: The University of Alberta Press 1981

Keith, C.M., Crampin, S.: Seismic body waves in anisotropic media: reflection and refraction at a plane interface. Geophys. J. **49**, 181–208, 1977a

Keith, C.M., Crampin, S.: Seismic body waves in anisotropic media: propagation through a layer. Geophys. J. **49**, 209–223, 1977b

Keith, C.M., Crampin, S.: Seismic body waves in anisotropic media: synthetic seismograms. Geophys. J. **49**, 225–243, 1977c

Kind, R.: Observations of sPn from Swabian Alb earthquakes at the GRF array. J. Geophys. **45**, 337–340, 1979

Matsumura, S.: Three-dimensional expression of seismic particle motions by the trajectory ellipsoid and its application to the seismic data observed in the Kanto district, Japan. J. Phys. Earth **29**, 221–239, 1981

Nuttli, O., Whitmore, J.D.: An observational determination of the variation of the angle of incidence of *P* waves with the epicentral distance. Bull. Seismol. Soc. Am. **51**, 269–276, 1961

Pho, H.-T., Behe, L.: Extended distances and angles of incidence of *P* waves. Bull. Seismol. Soc. Am. **62**, 885–902, 1972

Plešinger, A., Horálek, J.: The seismic broadband recording and data processing system FBV/DPS and its seismological applications. J. Geophys. **42**, 201–217, 1976

Plešinger, A.: Acquisition, processing and interpretation of broadband seismic data. In: Geophysical syntheses in Czechoslovakia, pp. 58–78. Bratislava: VEDA 1981

Rademacher, H., Odom, R.I., Kind, R.: The upper mantle structure under south-east Europe derived from broadband records of Greek earthquakes. J. Geophys. **52**, 7–13, 1983

Seidl, D.: The simulation problem for broad-band seismograms. J. Geophys. **48**, 84–93, 1980

Seidl, D., Stammler, W.: Restoration of broad-band seismograms (Part I). J. Geophys. **54**, 114–122, 1984

Received October 13, 1985; revised version December 9, 1985
Accepted December 10, 1985